Chapter 1

Raman spectroscopy for practical characterization of single-walled carbon nanotubes in various environments

Shohei Chiashi[1*], Yoshikazu Homma[2†] and Shigeo Maruyama[1,3‡]

[1] *Department of Mechanical Engineering, The University of Tokyo, Japan*
[2] *Department of Physics, Tokyo University of Science, Japan*
[3] *Energy NanoEngineering Laboratory, National Institute of Advanced Industrial Science and Technology (AIST), Tsukuba 305-8564, Japan*

Features of Raman scattering spectroscopy as a practical characterization tool of single-walled carbon nanotubes (SWCNTs) samples are reviewed. After the basic introduction of G-band, D-band, radial breathing mode (RBM), and 2D-band (G'-band) peaks, chirality dependent G^+, G^- features, doping effect, and resonance energy profiles are reviewed. Kataura plot; optical transition energy vs. RBM Raman shift; is the essential tool for the practical analysis of SWCNT sample. Available experimental data and correlation are summarized as the Kataura plot. The Raman shift and transition energy shift depending on SWCNT morphologies such as directly-grown sample on substrates, vertically-aligned sample, horizontally-aligned sample, suspended sample, and micelle-wrapped chirality-selected samples are compared. The detailed discussion of the environmental effect on Kataura plot follows. Finally, the temperature dependence of Raman features is discussed.

Contents

*chiashi@photon.t.u-tokyo.ac.jp
†homma@rs.tus.ac.jp
‡maruyama@photon.t.u-tokyo.ac.jp

2

Reminiscences of Millie

Raman spectroscopy of carbon nanotubes cannot be discussed without Millie. She has been the leader or the mentor of the initiation, development in experiment and in theory, and documentation of this research field. We have joined this exciting research field by the direct guidance of Millie. We witness that Millie was surprisingly kind and fair to new comers to the field. We can find so many researchers around the world who feel Millie as their direct mentor. Her initiatives, passion, and devote to science are always encouraging us and guiding us to continue research. We thank Millie for these immortal gifts.

1. Raman scattering spectra from SWCNTs

After the discovery of single-walled carbon nanotubes (SWCNTs),[1,2] Raman scattering spectroscopy is one of the most important analytical tools.[3] In Raman scattering spectra from SWCNT samples, the characteristic peaks appear and they come mainly from the phonon scattering. They are called the G-band, D-band, radial breathing mode (RBM) peaks, 2D-band (G'), and so on. The relevant phonons, Raman shift and scattering intensity of these peaks have been intensively studied. Hence, Raman scattering spectroscopy provides us plentiful information of SWCNTs. The knowledge is useful in analysis of not only SWCNTs but also the other carbon materials, especially nano-carbon materials, such as double-walled carbon nanotube, multi-walled carbon nanotube and graphene, and greatly contributes to the development of nanotechnology. The growth techniques of SWCNT samples have been proposed, such as arc-discharge methods,[1,2] laser-ablation method[4] and chemical vapor deposition methods,[5,6] and the growth techniques have developed rapidly. SWCNTs with various morphologies can be realized; directly-growth on substrates,[6] vertically-aligned growth,[7,8] horizontally-aligned growth[9] and suspended growth.[10] At the same time, separation techniques after the growth are also developed, and we can obtain even single chiraliry SWCNT samples.[11,12] As a result, the chirality dependence of their intrinsic physical properties are unveiled and it is found that they are affected by the morphology or the surrounding environments. The importance of Raman scattering spectroscopy is increasing for the detailed analysis of SWCNT samples. For example, Raman scattering spectra from SWCNTs, which were synthesized by using alcohol catalytic CVD (ACCVD) method,[13] are shown in Fig. 1. The G-band, which includes G^+ peak, G^- peak and BWF peak, D-band and RBM peaks are clearly observed. The split G-band is a characteristic feature of SWCNTs and RBM peaks are also unique to SWCNTs.

1.1. G-band

The G-band originates from an in-plane stretching mode of carbon-carbon bond in graphitic materials.[14] In graphite, since the G-band comes from phonons with

E_{2g} symmetry, which are equivalent longitudinal and transverse optical phonons at Γ point, the G-band appears as only one peak around $1580\,\mathrm{cm}^{-1}$. in the contrast to the single peak in the case of graphite or graphene, the G-band from SWCNTs appear around $1590\,\mathrm{cm}^{-1}$ as multiple peaks.[15] The G-band of SWCNTs composed of multiple peaks was explained to be the superposition of peaks from phonon with different symmetry, such as $2A$, $2E_1$ and $2E_2$ modes.[15] Even more complex G-band is often observed from bundled (aggregated) SWCNT samples.

Especially, two most prominent peaks among the G-band are called G$^+$ and G$^-$ peaks, and G$^-$ peak appears on the lower wavenumber side of G$^+$ peak. Raman scattering spectra are measured from not only bundled SWCNTs but also dispersed SWCNTs in solution[16] and suspended SWCNTs in air.[17] The G-band of single-chirality SWCNT is measured from chirality-separated SWCNT solutions or a single suspended SWCNT, and it generally exhibits only G$^+$ and G$^-$ peaks.[18] Because the theory states that the intensity of A mode peaks are strong,[19] the G$^+$ and G$^-$ are usually assigned to A symmetry phonons. The feature of G$^+$ and G$^-$ peaks from dispersed SWCNTs in solution are investigated in detail and it is found that the intensity ratio between G$^+$ and G$^-$ peaks depend on both d_{tube} and the chiral angle.[20]

In the case of semi-conducting SWCNTs, G$^+$ and G$^-$ peaks are sharp, and they originate from LO and TO phonons at Γ point, respectively. Raman shift of G$^+$ peak (ω_{G^+}) do not depend on the tube diameter (d_{tube}). On the other hand, that of G$^-$
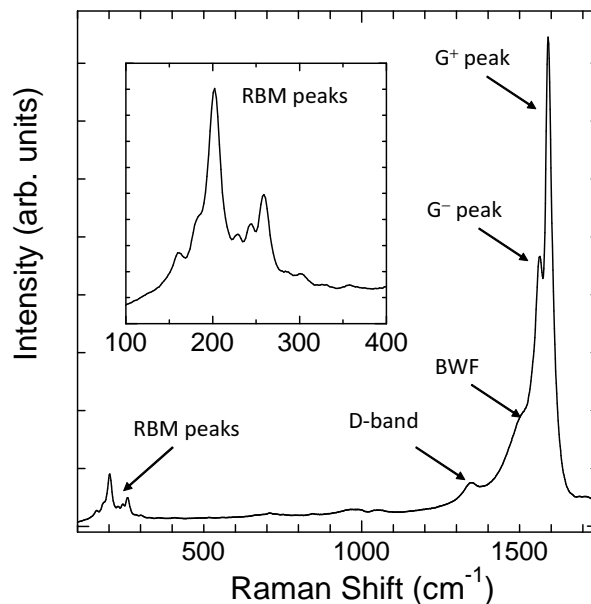

Fig. 1.   Raman scattering spectrum from SWCNTs, which were synthesized by using alcohol catalytic CVD (ACCVD) method.[13] The excitation laser wavelength was 488.0 nm ($E_{\mathrm{ex}} = 2.54\,\mathrm{eV}$).

4

peak (ω_{G^-}) clearly depend on the tube diameter, because of the curvature effect.[21] Therefore, the difference of their Raman shift ($\omega_{G^+} - \omega_{G^-}$) is roughly expressed by the tube diameter ($\omega_{G^+} - \omega_{G^-} = C_S/d_{\text{tube}}$, $C_S = 47.7\,\text{cm}^{-1}\text{nm}^2$).[22] In detail, ω_{G^-} depends on both the diameter and chiral angle,[23] as shown in Fig. 2(A).
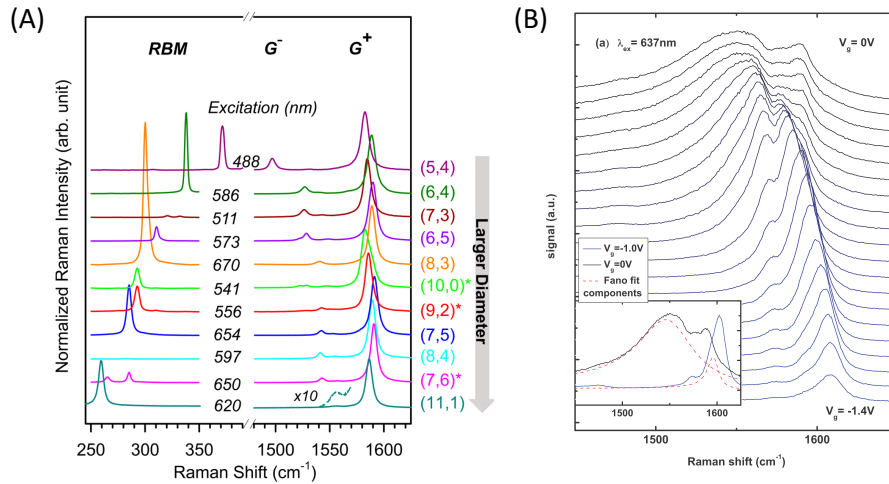

Fig. 2.   (A) G^+, G^- and RBM peaks of semi-conducting SWCNTs with different chirality, taken from Ref.([20]) with permission of Copyright © 2016, American Chemical Society. (B) G^+ and G^- peaks of metallic SWCNTs under the different gate voltage (V_g), taken from Ref.([24]) with permission of Benjamin Hatting, et al., *Phys. Rev. B*, **87**, 165442, 30 April 2013, Copyright by the American Physical Society.

For metallic SWCNTs, sharp G^+ and broad G^- peaks are observed and they correspond to TO and LO phonons at Γ point, respectively. Note that earlier reference imply G^+ and G^- peaks correspond to LO and TO phonons even for metallic SWCNTs, respectively. The LO phonon of metallic SWCNTs is softened due to Kohn anomaly,[25] and the softened and broad (asymmetric) G^- peak of metallic SWCNTs is also called Breit-Wigner-Fano (BWF) peak.[26] Because of the Kohn anomaly effect, the G-band of metallic SWCNTs is drastically modulated by changing the Fermi energy,[25,27,28] as shown in Fig. 2(B).

The density of states of SWCNTs exhibits almost discrete energy levels due to van Hove singularity and their optical transition energy (E_{ii}) corresponds to the energy gap between two energy states. Raman scattering spectra from SWCNTs are strongly enhanced by resonance Raman effect. If E_{ii} is equal to the energy of incident light (E_{ex}, incident resonance) or that of the scattered light ($E_{\text{ex}} \pm E_{\text{phonon}}$, scattered resonance), Raman scattering intensity becomes large. Here, $E_{\text{ex}} + E_{\text{phonon}}$ and $E_{\text{ex}} - E_{\text{phonon}}$ correspond anti-Stokes and Stokes scatterings,

respectively. Resonance Raman effect[29] is expressed by

$$I\left(E_{\mathrm{ex}}\right) \propto \left|\frac{1}{\left(E_{\mathrm{ex}} - E_{ii} + i\Gamma\right)\left(E_{\mathrm{ex}} \pm E_{\mathrm{phonon}} - E_{ii} + i\Gamma\right)}\right|^{2},$$ (1)

where Γ is a resonance window. Γ is a damping constant and is related to the finite lifetime of the intermediate state. In Raman excitation profiles of the G-band, two resonance peaks, which correspond to the incident and scattered resonances, clearly appear with $\Gamma = 26 - 43\,\mathrm{meV}$[30] for chirality-separated SWCNTs.
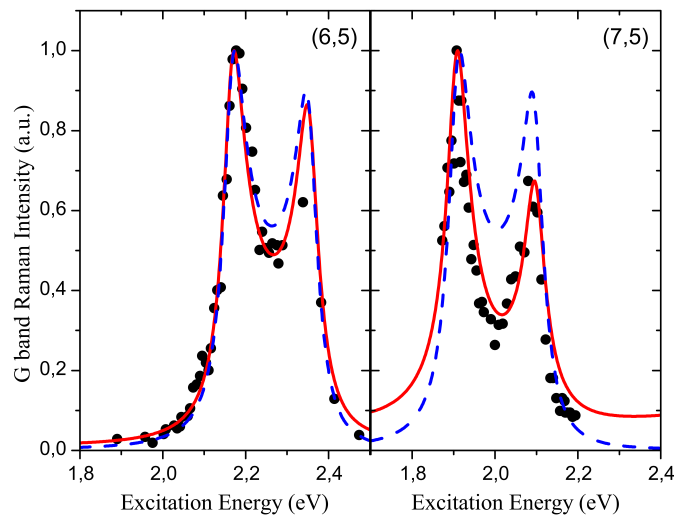

Fig. 3.   G-band resonance energy profile for $(6,5)$ and $(7,5)$ SWCNTs. The black circles are experimental data and the full red line is the present calculation with all matrix elements, while the dashed blue line is the same calculation using constant matrix elements. The electronic gap between the valence and conduction bands was corrected in a few electronvolts to fit with the experimental transitions.[31] Figure 3 is taken from Ref. ([31]) with permission of L. G. Moura, et al., *Phys. Rev. B*, **89**, 035402, 6 January 2014, Copyright by the American Physical Society.

Polarized Raman scattering spectroscopy is performed by using polarized incident and scattered lights, and it provides the information of the phonon symmetry, based on the group theory. The polarization effects of the G-band peaks have been reported.[15] In the case of SWCNTs, however, the resonance Raman effect and depolarization effects[32] due to the anisotropic geometry of SWCNTs are more prominent than the intrinsic polarization property of Raman scattering.[33] As a result, the intensity of the G-band is simply strong when the tube axis is parallel to the polarization of the incident and scattering light. The strong anisotropy is useful for analysis of the tube orientation of SWCNTs.[34]

Phonon vibration frequency and Raman shift are affected by isotope abundance. Although the natural abundance of ^{13}C carbon is constant $(1.1\,\%)$, it is possible to synthesize SWCNTs with arbitrary isotope abundance of carbon by using the

6

carbon source of ^{13}C.[35] Raman shift of ^{12}C and ^{13}C-SWCNTs is expressed by

$$\omega_{^{12}C_{(1-x)}{}^{13}C_x} = \omega_{^{12}C}\sqrt{\frac{m_{12}}{m_{12}(1-x)+m_{13}x}} \qquad (2)$$

where, $\omega_{^{12}C}$ is the phonon frequency of pure ^{12}C-SWCNT, and $\omega_{^{12}C_{(1-x)}{}^{13}C_x}$ is the phonon frequency of mixture of ^{12}C and ^{13}C-SWCNT, x is ^{13}C atom concentration, m_{12} and m_{13} are the mass of ^{12}C and ^{13}C carbon atoms, respectively. Equation (2) is available for G-band, D-band and 2D-band,[36] and the isotope abundance can be investigated by Raman scattering spectroscopy, as shown in Fig. 4.
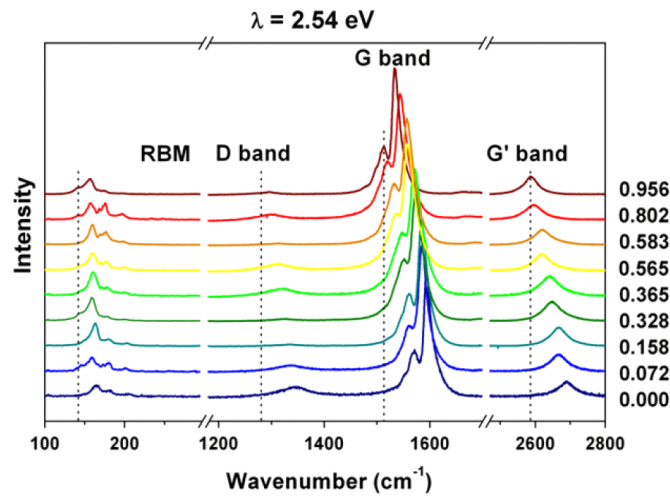

Fig. 4. Raman spectra of SWCNTS containing different amount of ^{13}C; RBM peaks, D-band, G-band and 2D-band spectral regions, taken from Ref. (^{36}) with permission of Elsevier.

1.2. D-band

The D-band is a defect-induced peak in graphitic structure and the D-band is explained by double resonance effect.[37,38] Therefore, the intensity ratio between the G-band and D-band is often used for the evaluation of crystallinity of graphitic structure for not only SWCNTs but also multi-walled carbon nanotube and other graphitic carbon materials. Tuinstra-Koening relation[14]

$$I_D/I_G = C(\lambda)/L_D, \qquad (3)$$

where, I_G and I_D are the intensity of the G-band and D-band, respectively, $C(\lambda)$ is the proportionality constant, which depends on the excitation laser wavelength, and L_D is the crystallite size, is used for characterization of the crystallinity of graphitic structure. In the case of graphene, L_D is estimated to be a few nm.[39]

While D-band is the defect-induced peak, it corresponds to a phonon around K point. Double resonance effect[37,38] involving scattering of phonon around K point

and inelastic scattering with defect structure, causes D-band peak. Because of the double resonance effect, Raman shift of the D-band (ω_{D}) shows the excitation light energy dependence ($d\omega_{\mathrm{D}}/dE_{\mathrm{ex}} \sim 53\,\mathrm{cm}^{-1}\mathrm{eV}^{-1}$).[38]

2D-band is the second-order Raman scattering of D-band phonon and it may be also called G'-band. It also appears due to double resonance effects.[37,38] In the case of 2D-band, inelastic scattering with defects is not required and 2D-band is observed from graphitic materials even without defect structure. Because no defect is involved, some people preferred to call as G'-band rather then 2D-band. The shape of the 2D-band of SWCNTs is different from that of double-walled carbon nanotubes (DWCNTs)[40] and the 2D-band is a signature for distinction between SWCNTs and DWCNTs.
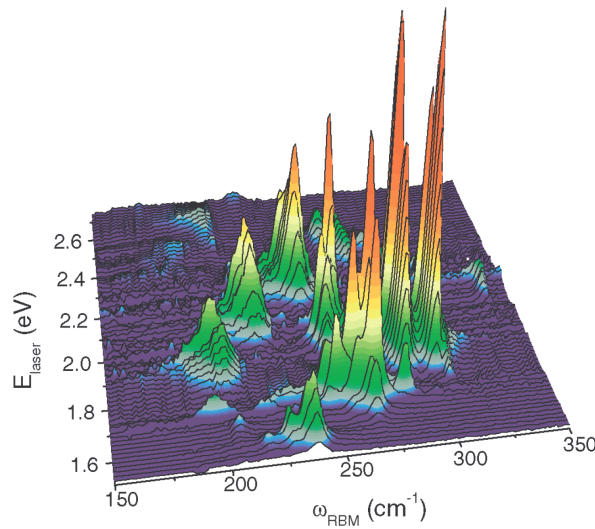
1.3. RBM peaks

Fig. 5.   RBM spectra of SDS-wrapped SWCNTs in solution, measured with 76 different laser lines, taken from Ref. ([41]) with permission of C. Fantini, et al., *Phys. Rev. Lett.*, **93**, 147406, 29 September 2004 Copyright by the American Physical Society. Each sharp peaks correspond to different chirality SWCNTs.

RBM peaks appear in the lower wavenumber region. Raman shift of RBM peaks (ω_{RBM}) is inversely proportional to its d_{tube},[42,43] as follows,

$$\omega_{\mathrm{RBM}} = A/d_{\mathrm{tube}}. \tag{4}$$

Therefore, RBM peaks are often used to analyze the d_{tube} distribution of SWCNT samples. However, as discussed in Sec. 2.1, ω_{RBM} is not exactly expressed by Eq. (4), because of the environmental effects on ω_{RBM}. Considering the environmental ef-

8

fects, the following equation,

$$\omega_{\mathrm{RBM}} = A/d_{\mathrm{tube}} + B \tag{5}$$

is often used. This simple equation is useful for analysis of SWCNT tube diameter, although the values of A and B vary depending the environments, as discussed in Sec. 2.1.
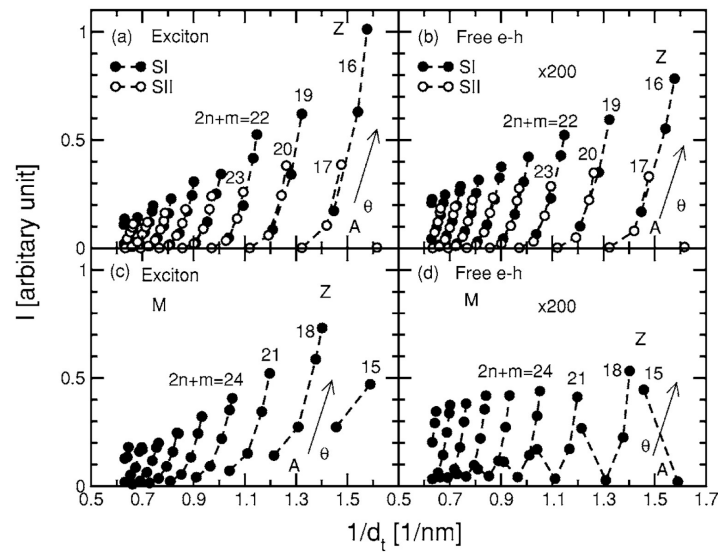

Fig. 6.   RBM Raman intensity per length for SWCNTs with $0.6 < d_{\mathrm{tube}} < 1.6\,\mathrm{nm}$.(a) and (b) are for E_{22} $\left(A_2^0\right)$ and free e-h at k_{22} in semiconducting-SWCNTs, respectively. Filled and open circles are for SI and SII tubes. (c) and (d) are for $E_{11\mathrm{L}}$ $\left(A_2^0\right)$ and free e-h at $k_{11\mathrm{L}}$ in metallic SWCNTs, respectively. The intensity in the free el-ph case has been multiplied by 200. The arrows indicate the θ decreasing direction (A, armchair side; Z, zigzag side). In (d), within a family the armchair tube has a larger intensity than its neighbor due to a node effect. Figure 6 is taken from Ref. ([44]) with permission of J. Jiang, et al., *Phys. Rev. B*, **75**, 035405, 8 January 2007, Copyright by the American Physical Society.

RBM peaks are strongly enhanced by resonance Raman effect and the resonance Raman effect is also expressed by Eq. (1). As shown in Fig. 5, spectra of RBM peaks change with changing the excitation wavelength. Each peaks come from different chirality and the intensity also clearly depend on the chirality. In general, SWC-NTs with smaller chiral angle (near zigzag) exhibit stronger intensity of the RBM peaks,[44] as shown in Fig. 6. Additionally, the relationship between the intensity of G^+ and RBM peaks is investigated for chirality-separated SWCNT samples and it shows the chirality dependence.[20]

1.4. *Kataura plots*

As mentioned above, the intensity of RBM peaks is strongly enhanced by resonance Raman scattering effect. The phonon energy of RBM peaks is approximately a few tens of milli electronvolts. When E_{ex} is in visible or infrared range, E_{phonon} of RBM peaks is quite small compared with E_{ex}. Therefore, it is usually impossible to distinguish the incident and scattered resonances (Eq. (1)) and only E_{ii} is simply regarded as the resonance energy in RBM peaks.

The relationship between ω_{RBM} and E_{ii} is called Kataura plot.[49] Figure 7 shows an example of Kataura plot, which is a compilation of experimental data.[41,45–48] Because both ω_{RBM}[42,43] and E_{ii}[50] are roughly proportional to $1/d_{\mathrm{tube}}$, the plots in Fig. 7 appear along lines from the lower left to the top right. Here, the E_{ii}^{S} and E_{ii}^{M} are the i-th optical transition energy of semi-conducting and metallic SWCNTs, respectively. In Fig. 7, five different optical transition energies are shown, such as
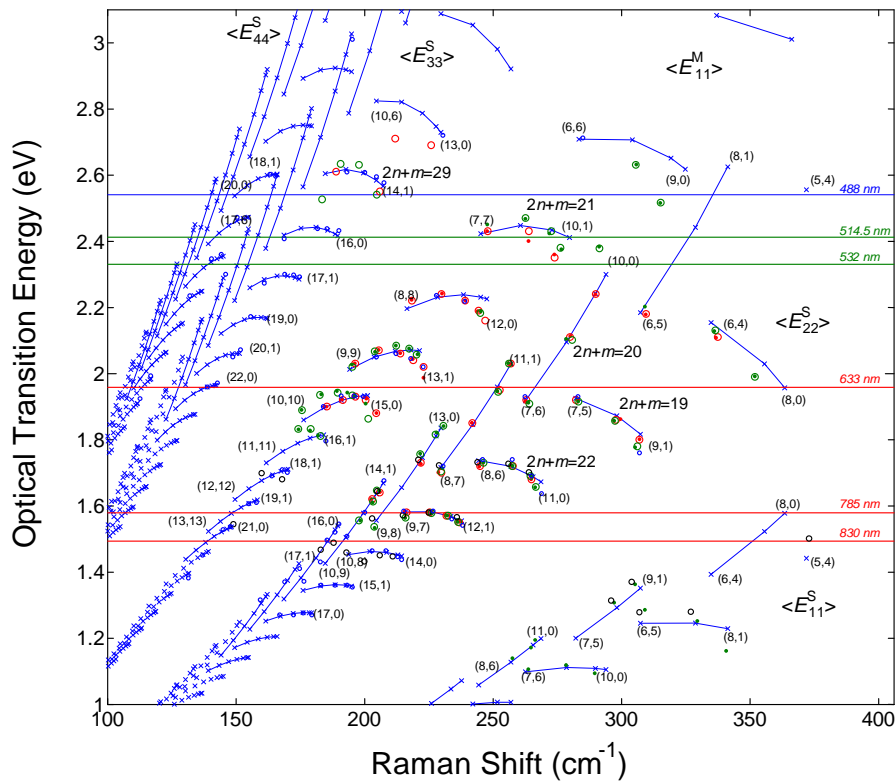
Fig. 7.   Empirical Kataura plots of SWCNTs. Blue open circles (○)[45] are measured from as-grown SWCNTs. Blue cross marks (×) are calculated from the empirical equation.[45] Green open circles (○),[46] red open circles (○) [41] and filled circle (●) [47] are measured from dispersed SWCNTs in solution. Green filled circles (●)[48] are measured from suspended SWCNTs. The energy of excitation laser, which is widely used for Raman scattering measurement of SWCNTs, is shown.

10

E_{11}^{S}, E_{11}^{M}, E_{22}^{S}, E_{33}^{S} and E_{44}^{S}. E_{ii} depends on both d_{tube} and the chiral angle (θ). Therefore, the plots do not appear just along lines and slightly spread. In Fig. 7, the plots with the same value of $(2n+m)$ are connected with line segments and they show so-called "family pattern".[51] Some of the plots are shown with chiral index (n, m) or the number of $(2n + m)$. Semi-conducting SWCNTs are often categolized into two groups. Semi-conducting SWCNTs with $(2n + m)$ mod $3 = 1$ and 2 are called 'type-I' ('SI' or 'mod2') and 'type-II' ('SII' or 'mod1') SWCNTs, respectively. Some properties of SWCNTs show the type-dependence. For example, E_{ii} depends on strain and whether E_{ii} increases or decreases is determined by the type.[52]

Based on Kataura plot, it is possible to assign the chirality from measured RBM peaks. When E_{ii} is close to the E_{ex}, the RBM peaks are observed. The resonance window (Γ) depend on SWCNT samples, such as SDS wrapped SWNTs in solution ($\Gamma = 60\,\mathrm{meV}$) and bundled SWCNTs ($\Gamma = 120\,\mathrm{meV}$).[41] According to Kataura plots, for example, RBM peaks in Fig. 1 correspond to semiconducting SWCNTs with $2n + m = 29$ and metallic SWCNTs with $2n + m = 21$.

2. Environmental effects on Kataura plots

The plots of some typical SWCNT samples, such as as-grown SWCNT,[45] which may be bundled, surfactant-wrapped SWCNTs in water solution,[46] and suspended in air,[48] are shown in Fig. 7. Although these plots are slightly different, they show a similar feature. Note that the blue cross marks are calculated from the empirical equation.[45]

Additionally, two more kinds of SWCNTs, which are vertically-aligned SWCNTs and suspended SWCNTs in vacuum, are considered and their plots are added in Kataura plot in Fig. 8. These two kinds of SWCNTs are clearly different from former SWCNT samples. ω_{RBM} and E_{ii} considerably change depending on the surrounding condition around SWCNTs, which is called "environmental effects". In the following, the environmental effects on ω_{RBM} and E_{ii} are discussed.

2.1. *Raman shift*

d_{tube} is geometrically defined by the chirality index (n, m) with the lattice constant ($a_{\mathrm{C-C}}$) of the honeycomb structure of carbon atoms, as follows

$$d_{\mathrm{tube}} = \sqrt{3}a_{\mathrm{C-C}}\frac{\sqrt{n^2 + nm + m^2}}{\pi}. \tag{6}$$

$a_{\mathrm{C-C}}$ of graphene is 0.142 nm and the value of $a_{\mathrm{C-C}} = 0.142\,\mathrm{nm}$ is also used for SWCNTs.[55] Note that the value of $a_{\mathrm{C-C}} = 0.144\,\mathrm{nm}$ has often been employed for the calculation of SWCNT diameter.[56] Density functional theory calculation reveals that $a_{\mathrm{C-C}}$ depends on d_{tube} in small d_{tube} range and $a_{\mathrm{C-C}}$ increases with decreasing d_{tube}.[57] $a_{\mathrm{C-C}}$ of SWCNTs with 0.6 nm in diameter is approximately 0.144 nm. However, typical d_{tube} of SWCNTs, which are synthesized experimentally, is 0.7 nm at the smallest (for example $(6, 5)$ SWCNT). For simple comparison, the coefficients

of the equations, such as A in Eq. (4), or A and B in Eq. (5), are re-calculated by using the $a_{C-C} = 0.142\,\mathrm{nm}$ instead of $a_{C-C} = 0.144\,\mathrm{nm}$.

ω_{RBM} is simply proportional to $1/d_{tube}$,.[42,43] With given the speed of sound in SWCNTs, theory predicts that the value of A is $227\,\mathrm{cm^{-1}nm}$.[42] In fact, in the case of suspended and isolated SWCNTs in vacuum, the value of A is measured to be $227\,\mathrm{cm^{-1}nm}$[54] or $228\,\mathrm{cm^{-1}nm}$.[58] Because suspended SWCNTs in vacuum are perfectly free, they exhibit their intrinsic properties. In isolated and suspended SWCNTs, experimental and theoretical results show good agreement of the diameter dependence of ω_{RBM}. The same value of A ($227\,\mathrm{cm^{-1}nm}$) is obtained from vertically-aligned SWCNTs.[59] Hence, vertically-aligned SWCNTs are directly grown on substrates. They vertically stand up on the substrate with entangling each other, and form the small-bundle structure.[60] The value of $A = 227\,\mathrm{cm^{-1}nm}$ suggests that partially-suspended and isolated SWCNTs exist in vertically-aligned SWCNT samples and they are not covered with any substances.

Generally, as-grown SWCNTs are bundled or interacting with other materials. Therefore, in order to express the relationship between ω_{RBM} and d_{tube}, various values of A had been reported. $A = 244.6\,\mathrm{cm^{-1}nm}$ ($A = 248\,\mathrm{cm^{-1}nm}$ with $a_{C-C} = 0.144\,\mathrm{nm}$ in the original literature)[61] was obtained from SWCNTs grown on silicon substrates and $A = 223.75\,\mathrm{cm^{-1}nm}$ was from bundled SWCNT samples.[62]

As the other type of approximation to express the environmental effects on ω_{RBM}, Eq. (5) is frequently used. The value of B express the "environmental effect" on ω_{RBM}, and many combination of the values (A, B) is proposed
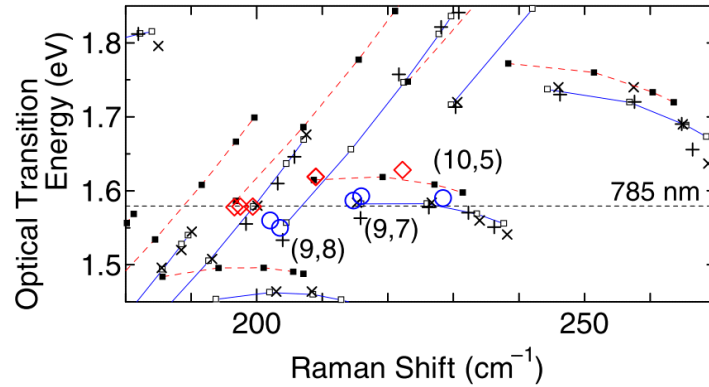

Fig. 8.   Relationship between ω_{RBM} and the E_{ii} (Kataura plot) obtained from suspended SWC-NTs. The PL and Raman scattering measurements were performed in vacuum (open diamond, $\lozenge$) and water vapor (open circle, $\circ$). The plots of as-grown SWCNTs $(\times)$[45] and surfactant wrapped SWCNTs in solution $(+)$[46] are shown as reference. The open $(\square)$[45] and filled square $(\blacksquare)$[53] marks present the Raman resonant energy and ω_{RBM}, which are calculated from the empirical equations for as-grown and vertically aligned SWCNT samples, respectively. Figure 8 is taken from Ref. ([54]) with permission of S. Chiashi, et al., *Phys. Rev. B*, **91**, 155415, 15 April 2015, Copyright by the American Physical Society.
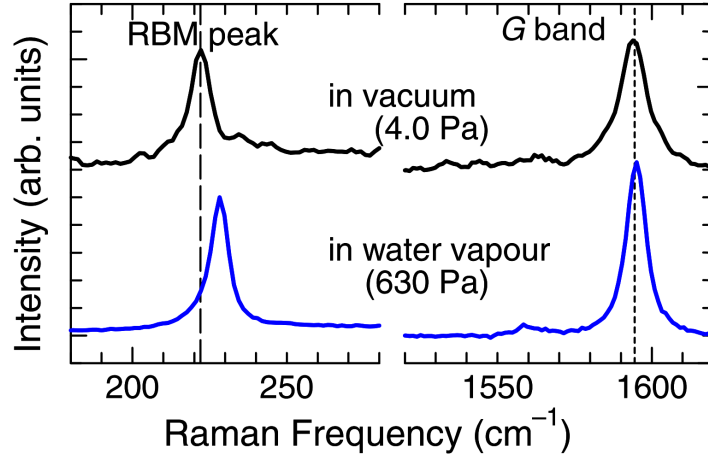
12

Fig. 9. Raman scattering spectra (G-band and RBM peak) from $(10, 5)$ SWCNT, measured in vacuum $(4.0\,\text{Pa})$ and water vapor $(630\,\text{Pa})$. The wavelength of the excitation laser is $785\,\text{nm}$. Figure 9 is taken from Ref. (^{63}) with permission of Y. Homma, et al., *Phys. Rev. Lett.*, **110**, 157402, 9 April 2013, Copyright by the American Physical Society.

for various SWCNT samples. For example, $(A, B) = (220.4, 12.5)$ [$(223.5, 12.5)$ with $a_{\text{C}-\text{C}} = 0.144\,\text{nm}$ in the original literature],[64] $(218, 17)$ for metallic SWC-NTs and $(223, 10)$ for semi-conducting SWCNTs,[41] $(214.4, 18.7)$,[65] $(215, 18)$[66] and $(217.8, 15.7)$[45] are measured from SDS-wrapped SWCNTs. $(A, B) = (204, 27)$[67] is reported for suspended SWCNTs and the value of B is non-zero in spite of suspended SWCNTs. The non-zero value of B suggests that the suspended SWCNTs are adsorbed with water layer and the adsorption effects modified ω_{RBM},[54] as discussed later. Equation (5) is also available for the case of suspended SWCNTs in vacuum with $(A, B) = (227, 0)$ or $(228, 0)$, and it is practically useful for investigation of RBM peaks and estimation of the tube diameter distribution of SWCNTs, although the available surrounding conditions and diameter range should be considered. Note that A and B are simply fitting parameters and they do not have physical meanings.

In order to investigate the environmental effect on ω_{RBM}, some models are proposed. One is a model, where SWCNT is surrounded by an environmental shell and it is under inward pressure.[59] In this model,

$$\omega_{\text{RBM}} = (A/d_{\text{tube}}) \sqrt{1 + C * d_{\text{tube}}^2} \qquad (7)$$

where

$$C = \frac{6\left(1 - \nu^2\right)}{Eh} \frac{K}{s_0{}^2} \qquad (8)$$

is obtained, where ν is the Poissons ratio, E is the Youngs modulus, h is the thickness of the SWCNT wall, K is the van der Waals interaction strength, and

s_0 is is the equilibrium separation between the SWCNT wall and the environment shell. In Eq. (7), the values of $(A, C) = (227, 0.05786)$[59] are available for various SWCNT sample. Of course, Eq. (7) with $(A, C) = (227, 0)$ is available for suspended SWCNTs in vacuum.[59]

Other one is a model, where SWCNT is wrapped with surrounding media. Assuming that the surrounding media physically adsorb on the outer surface of SWCNTs, the interaction between the SWCNT and the media is regarded to be the van der Waals interaction and the mechanical coupling of radial breathing vibration between SWCNT and the surrounding media causes the environmental effect on ω_{RBM}.[54] $\omega_{\mathrm{RBM}}^{\mathrm{in}}(= A/d_{\mathrm{tube}})$ is the intrinsic RBM frequency of SWCNT, ω_{ad} is the vibration frequency of radial breathing mode of the surrounding media and $\omega_{\mathrm{RBM}}^{\mathrm{ex}}$ is the extrinsic frequency due to the environmental effects. Based on simple dynamic considerations, the dynamical matrix is

$$\begin{bmatrix} (\omega_{\mathrm{ad}})^2 + K_{11} & K_{12} \\ K_{21} & \left(\omega_{\mathrm{RBM}}^{\mathrm{in}}\right)^2 + K_{22} \end{bmatrix} \tag{9}$$

and the matrix gives $\omega_{\mathrm{RBM}}^{\mathrm{ex}}$ as the eigenvalue. K_{ij} is the interaction between SWCNT and the surrounding media and they are calculated by integration of the interaction between the carbon atoms and atoms of the surrounding media. In this model, the environmental effects of SWCNTs (bundle structure) and water adsorption layer as the surrounding media can be calculated with the value of $A = 227\,\mathrm{cm}^{-1}\mathrm{nm}$, and the calculated results show good agreement with the experiments for wide d_{tube} range.[54] RBM peak from suspended $(10, 5)$ SWCNT measured in vacuum and water vapor are shown in Fig. 9. Sharp single RBM peak clearly appears and the peak is up-shifted in water vapor. The up-shift comes from the adsorption of water molecules on the outer surface of SWCNT. Since the interaction between water and SWCNT is not so strong, strain or inward pressure do not occur in suspended SWCNT.

SWCNTs lying on substrates are one of the most typical SWCNT samples. and their ω_{RBM} are affected by contact with substrates. However, the substrate effect on ω_{RBM} is complicate, because the substrate contact is not axial symmetry, the radical deformation may affect[68] and the interaction between SWCNTs and substrates is very diverse. By using suspended SWCNTs over the trench structure, the substrate effect is investigated and ω_{RBM} of supported parts, which is in contact with the substrate, is a few cm^{-1} higher than that of suspended parts.[69] Axial strain also affects ω_{RBM} and 10% tensile strain causes up-shift by a few cm^{-1}.[70]

2.2. *Resonance energy*

In order to determine the resonance Raman energy, Raman scattering spectra are measured by continuously changing the wavelength of excitation light.[41] Usually, laser source is used as the excitation light and the different optical systems for each wavelength are needed. Therefore, it is not so easy to measure the resonance
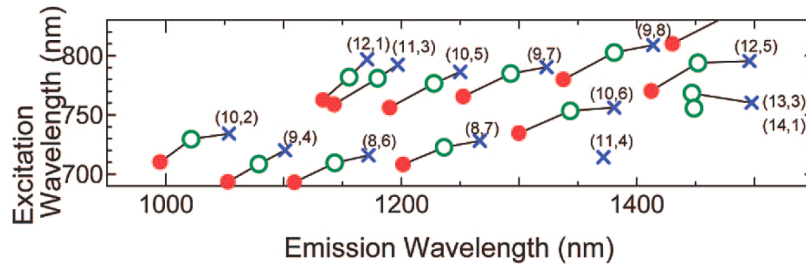
14

Fig. 10. Emission and excitation wavelengths of surfactant-wrapped SWCNTs ($\times$), suspended SWNTs in air ($\circ$) and suspended SWCNTs in vacuum ($\bullet$).[71] While no substance adsorb on the suspended SWCNTs in vacuum, water molecules adsorb on the outer surface of suspended SWCNTs in air. Figure 10 is taken from Ref. ([71]) with permission of Copyright © 2008, American Chemical Society.

Raman energy. On the other hand, photoluminescence (PL) spectroscopy is useful tool to measure E_{ii} although PL emission is measured from only semi-conducting SWCNTs. Only by changing the excitation wavelength, PL spectroscopy gives us the information of E_{ii}.[64] Additionally, it is reported that Raman excitation profiles of RBM peaks is almost the same as PL emission spectra.[72] Here, assuming that the resonance Raman energy of RBM peaks is simply equal to E_{ii} which are obtained by PL spectroscopy, the environmental effects of the resonance Raman energy is discussed.

E_{ii} is not simply the energy difference between a pair of van Hove singularity peaks in the electronic density of states of SWCNTs. The interaction between excited electron and hole, and between excited electron and the other electrons should be considered and these interactions determine the binding energy of exciton. The binding energy of exciton of SWCNTs is relatively large and the binding energy contributes to E_{ii}.[73] The binding energy depends on the dielectric constant, ϵ because the Coulomb interaction is a function of ϵ. The dielectric constant is affected by the surrounding condition of SWCNTs and it is the one of the origin of the environmental effects of E_{ii}. Usually, in the case of SWCNTs, E_{ii} decreases with increasing the dielectric constant.[73]

As mentioned in Sec. 2.1, suspended SWCNTs in vacuum are perfectly free from any substances and they show the intrinsic property of SWCNTs. Their E_{ii} are measured by PL spectroscopy and the value of E_{ii} is larger than those in the other conditions,[71] as shown in Fig. 10. E_{11} and E_{22} of suspended SWCNTs in vacuum are clearly larger than those of suspended SWCNTs in air, which are adsorbed with water layer, and surfactant-wrapped SWCNTs. The same value of E_{ii} is obtained from vertically-aligned SWCNTs.[74] It also suggests the existence of partially suspended and isolated SWCNTs in vertically-aligned SWCNT samples. The environmental effect on E_{ii} is investigated by the immersion of suspended SWCNTs into various liquids.[75] SWCNTs exhibit different E_{ii} depending on the dielectric constant of liquids.

Additionally, the interaction among SWCNTs in bundle structure decreases E_{ii} and increase the resonance Raman window (Γ).[41] Γ of SDS-wrapped SWCNTs is 65 meV, while that of bundled SWCNT is 112 meV.[41] The similar bundling effects on E_{ii} is measured by PL spectroscopy.[76]

Strain changes E_{ii} and the shift of E_{ii} shows type-dependence.[52,77] Small band gap appears in metallic SWCNTs due to strain. Whether E_{ii} of semi-conducting SWCNTs increases or decreases depends on the value of $p = (n - m) \mod 3$

$$\Delta E = \mathrm{sgn}\,(2p + 1)\, 3t_0 \left[(1 + \nu)\, \sigma \cos 3\theta + \gamma \sin 3\theta\right] \tag{10}$$

where $p = 1$ or $p = -1$ is for type-I or type-II, respectively, t_0 is the tight-binding overlap integral, ν is the Poisson's ratio, σ and γ are uniaxial and torsional strains, respectively.[52]

2.3. *Temperature dependence*

Raman scattering spectra depend on temperature. It is well-known that the intensity ratio between Stokes and anti-Stokes scattering is a function of temperature, as follows

$$\frac{I_{\mathrm{AS}}}{I_{\mathrm{S}}} = \exp\left(-\frac{E_{\mathrm{phonon}}}{k_{\mathrm{B}} T}\right) \tag{11}$$

where, I_{S} and I_{AS} are the intensity of Stokes and anti-Stokes scattering, k_{B} is the Boltzmann constant, and T is temperature. It is generally possible to obtain the phonon temperature from the intensity ratio. However, in the case of the G-band of SWCNTs, Eq. (11) is not valid. The G-band intensity is strongly enhanced by resonance Raman effect and the phonon energy of the G-band (approximately 0.2 eV) is relatively large. Therefore, the scattered resonance energy is different between Stokes and anti-Stokes ($E_{\mathrm{ex}} \pm E_{\mathrm{phonon}}$) and Raman excitation profiles are also different.[41]

Although Eq. (11) is not available for the G-band, it is possible to measure the SWCNT temperature from Raman shift of the G-band. Generally, with increasing temperature, Raman shift decreases and the peak width increases because of nonharmonic component of lattice vibration. Raman shift of the G-band decreases with increasing temperature [78] [79] and the temperature dependence of the G^+ peak is simply expressed by[80]

$$\omega_{\mathrm{G}^+}\,(T) = \omega_0 - \frac{a}{\exp\,(b\hbar\omega_0/k_{\mathrm{B}}T) - 1} \tag{12}$$

where $h\,(= 2\pi\hbar)$ is the Planck constant and a, b and ω_0 are fitting parameters. $a = 38.4\,\mathrm{cm}^{-1}$, $b = 0.438$ and $\omega_0 = 1594\,\mathrm{cm}^{-1}$ are valid in the wide temperature range (form 0 to 1000 K).[80] In Fig. 11, the temperature dependence of ω_{G^+} measured from different SWCNT samples and the curve calculated by Eq. (12) are shown.

In Kataura plot, the temperature dependence is important, because both ω_{RBM} and E_{ii} depend on temperature. RBM peaks exhibit downshift of Raman shift and broadening of peak and E_{ii} also decrease width with increasing temperature.[41,81]
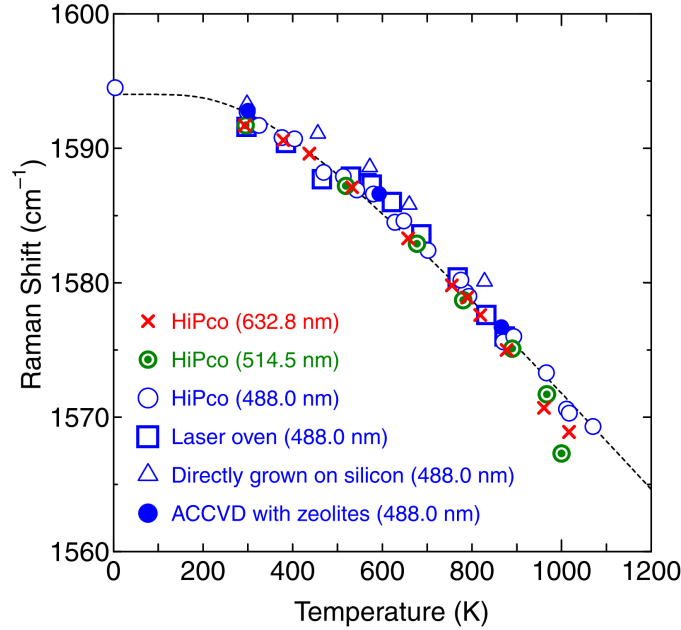
16

Fig. 11.   Temperature dependence of Raman shifts of G^+ peaks for various SWNT samples measured with a 488.0 nm excitation laser and for HiPco sample measured with three excitation lasers (488.0, 514.5, and 632.8 nm). The dashed line is a fitting line calculated using Eq. (12). The graph is taken from Ref.[80]

The temperature dependence of E_{ii} of semi-conducting SWCNTs is investigated by PL spectroscopy,[82] and the energy shift of E_{ii} (ΔE_{ii}) is expressed by Varshni equation, as follows

$$\Delta E_{ii}\left(T\right) = -\frac{\alpha T^2}{T + \beta} \tag{13}$$

where, α and β are the constants. While $\alpha = 0.075\,\mathrm{meV/K}$ and $\beta = 600\,\mathrm{K}$ are obtained in the case of E_{11} of suspended $(12, 2)$ SWCNT in lower temperature range,[82] $\alpha = 0.177\,\mathrm{meV/K}$ and $\beta = 1800\,\mathrm{K}$ are measured from suspended SWCNTs with various chiralities in the higher temperature range.[83] The temperature dependence of ω_{RBM} is also reported. The obtained values of $\partial\omega_{\mathrm{RBM}}/\partial T$ are diverse, such as $\partial\omega_{\mathrm{RBM}}/\partial T = -0.013$ and $-0.015\,\mathrm{cm}^{-1}/\mathrm{K}$,[84] -0.0045 and $-0.009\,\mathrm{cm}^{-1}/\mathrm{K}$,[78] $\sim 0.006\,\mathrm{cm}^{-1}$,[79] and $-0.001 \sim -0.015\,\mathrm{cm}^{-1}/\mathrm{K}$.[80]

Temperature increase often occurs during Raman scattering measurement. The optical absorption cross-section of SWCNTs is a few $10 \times 10^{18}\,\mathrm{cm}^2/\mathrm{atom}$ at the E_{ii} (on-resonance).[85] The temperature of SWCNTs under light irradiation is determined by the power density of excitation light, the light absorption cross-section, the thermal conductivity and the thermal conductance between SWCNTs and the surrounding system. Especially, the temperature of SWCNTs is easily increased in the cases of SWCNTs in vacuum, on substrates with low thermal conductivity and

suspended SWCNTs. During the measurement in atmospheric ambient, it is possible that SWCNTs under light irradiation are damaged or burned by oxidization. Even without damage, the temperature dependence of E_{ii} and ω_{RBM} could appear in RBM spectra.

3. Acknowledgments

References

1. S. Iijima and T. Ichihashi, Single-shell carbon nanotubes of 1-nm diameter, *Nature.* **363**, 603–605, (1993).
2. D. S. Bethune, C. H. Kiang, M. S. de Vries, G. Gorman, R. Savoy, J. Vazquez, and R. Beyers, Cobalt-catalysed growth of carbon nanotubes with single-atomic-layer walls, *Nature.* **363**, 605–607, (1993).
3. A. M. Rao, E. R. S. Bandow, B. C. P. C. Eklund, K. A. Williams, S. Fang, K. R. Subbaswamy, M. Menon, A. Thess, R. E. Smalley, G. Dresselhaus, and M. S. Dresselhaus, Diameter-selective Raman scattering from vibrational modes in carbon nanotubes, *Science.* **275**, 187–191, (1997).
4. A. Thess, R. Lee, P. Nikolaev, H. J. Dai, P. Petit, J. Robert, C. H. Xu, Y. H. Lee, S. G. Kim, A. G. Rinzler, D. T. Colbert, G. E. Scuseria, D. Tomanek, J. E. Fischer, and R. E. Smalley, Crystalline ropes of metallic carbon nanotubes, *Science.* **273**, 483–487, (1996).
5. H. Dai, A. G. Rinzler, P. N. Nikolaev, A. Thess, D. T. Colbert, and R. E. Smalley, Single-wall nanotubes produced by metal-catalyzed disproportionation of carbon monoxide, *Chem. Phys. Lett.* **260**, 471–475, (1996).
6. J. Kong, H. T. Soh, A. M. Cassell, C. F. Quate, and H. J. Dai, Synthesis of individual single-walled carbon nanotubes on patterned silicon wafers, *Nature.* **395**, 878–881, (1998).
7. Y. Murakami, S. Chiashi, Y. Miyauchi, M. H. Hu, M. Ogura, T. Okubo, and S. Maruyama, Growth of vertically aligned single-walled carbon nanotube films on quartz substrates and their optical anisotropy, *Chem. Phys. Lett.* **385**, 298–303, (2004).
8. K. Hata, D. N. Futaba, K. Mizuno, T. Namai, M. Yumura, and S. Iijima, Water-assisted highly efficient synthesis of impurity-free single-walled carbon nanotubes, *Science.* **306**, 1362–1364, (2004).
9. A. Ismach, L. Segev, E. Wachtel, and E. Joselevich, Atomic-step-templated formation of single wall carbon nanotube patterns, *Angew. Chem. Int. Ed.* **43**, 6140–6143, (2004).
10. A. M. Cassell, N. R. Franklin, T. W. Tombler, E. M. Chan, J. Han, and H. J. Dai, Directed growth of free-standingsingle-walled carbon nanotubes, *J. Am. Chem. Soc.* **121**, 7975–7976, (1999).
11. M. S. Arnold, A. A. Green, J. F. Hulvat, S. I. Stupp, and M. C. Hersam, Sorting carbon nanotubes by electronic structure using density differentiation, *Nat. Nanotechnol.* **1**, 60–65, (2006).

18

12. X. Tu, S. Manohar, A. Jagota, and M. Zheng, DNA sequence motifs for structure-specific recognition and separation of carbon nanotubes, *Nature.* **460**, 250–253, (2009).

13. S. Maruyama, R. Kojima, Y. Miyauchi, S. Chiashi, and M. Kohno, Low-temperature synthesis of high-purity single-walled carbon nanotubes from alcohol, *Chem. Phys. Lett.* **360**, 229–234, (2002).

14. F. Tuinstra and J. L. Koenig, Raman spectrum of graphite, *J. Chem. Phys.* **53**, 1126–1130, (1970).

15. A. Jorio, M. A. Pimenta, A. G. Souza, G. G. Samsonidze, A. K. Swan, M. S. Unlu, B. B. Goldberg, R. Saito, G. Dresselhaus, and M. S. Dresselhaus, Resonance Raman spectra of carbon nanotubes by cross-polarized light, *Phys. Rev. Lett.* **90**, 107403–1–107403–4, (2003).

16. S. Lebedkin, F. Hennrich, T. Skipa, and M. M. Kappes, Near-infrared photolumines-cence of single-walled carbon nanotubes prepared by the laser vaporization method, *J. Phys. Chem. B.* **107**, 1949–1956, (2003).

17. Y. Kobayashi, T. Yamashita, Y. Ueno, O. Niwa, Y. Homma, and T. Ogino, Extremely intense Raman signals from single-walled carbon nanotubes suspended between Si nanopillars, *Chem. Phys. Lett.* **386**, 153–157, (2004).

18. H. B. Son, Y. Hori, S. G. Chou, D. Nezich, G. G. Samsonidze, G. Dresselhaus, M. S. Dresselhaus, and E. B. Barros, Environment effects on the Raman spectra of individual single-wall carbon nanotubes: Suspended and grown on polycrystalline silicon, *Appl. Phys. Lett.* **85**, 4744–4746, (2004).

19. V. Avramenko and S. B. Rochal, Symmetry of the carbon nanotube modes and their origin from the phonon branches of graphene, *Phys. Rev. B.* **87**, 035407–1–035407–8, (2013).

20. Y. Piao, J. R. Simpson, J. K. Streit, G. Ao, M. Zheng, J. A. Fagan, and A. R. H. Walker, Intensity ratio of resonant Raman modes for (n, m) enriched semiconducting carbon nanotubes, *ACS Nano.* **10**, 5252–5259, (2016).

21. X. Blase, L. X. Benedict, E. L. Shirley, and S. G. Louie, Hybridization effects and metallicity in small radius carbon nanotubes, *Phys. Rev. Lett.* **72**, 1878–1881, (1994).

22. A. Jorio, A. G. Souza, G. Dresselhaus, M. S. Dresselhaus, A. K. Swan, M. S. Unlu, B. B. Goldberg, M. A. Pimenta, J. H. Hafner, C. M. Lieber, and R. Saito, G-band resonant Raman study of 62 isolated single-wall carbon nanotubes, *Phys. Rev. B.* **65**, 155412–1–155412–9, (2002).

23. H. Telg, J. G. Duque, M. Staiger, X. Tu, F. Hennrich, M. M. Kappes, M. Zheng, J. Maultzsch, C. Thomsen, and S. K. Doorn, Chiral index dependence of the G^+ and G^- Raman modes in semiconducting carbon nanotubes, *ACS Nano.* **6**, 904–911, (2012).

24. B. Hatting, S. Heeg, K. Ataka, J. Heberle, F. Hennrich, M. M. Kappes, R. Krupke, and S. Reich, Fermi energy shift in deposited metallic nanotubes: A Raman scattering study, *Phys. Rev. B.* **87**, 165442–1–165422–5, (2013).

25. H. Farhat, H. Son, G. Samsonidze, S. Reich, M. Dresselhaus, and J. Kong, Phonon softening in individual metallic carbon nanotubes due to the Kohn anomaly, *Phys. Rev. Lett.* **99**, 145506–1–145506–4, (2007).

26. S. D. M. Brown, A. Jorio, P. Corio, M. S. Dresselhaus, G. Dresselhaus, R. Saito, and K. Kneipp, Origin of the Breit-Wigner-Fano lineshape of the tangential G-band feature of metallic carbon nanotubes, *Phys. Rev. B.* **63**, 155414–1–155414–8, (2001).

27. J. S. Park, K. Sasaki, R. Saito, W. Izumida, M. Kalbac, H. Farhat, G. Dresselhaus, and M. S. Dresselhaus, Fermi energy dependence of the G-band resonance Raman spectra of single-wall carbon nanotubes, *Phys. Rev. B.* **80**, 081402(R)–1–081402(R)–4, (2009).

28. K. Nguyen, A. Gaur, and M. Shim, Fano lineshape and phonon softening in single

isolated metallic carbon nanotubes, *Phys. Rev. Lett.* **98**, 145504–1–145504–4, (2007).

29. M. A. Pimenta, A. Marucci, S. A. Empedocles, M. G. Bawendi, E. B. Hanlon, A. M. Rao, P. C. Eklund, R. E. Smalley, G. Dresselhaus, and M. S. Dresselhaus, Raman modes of metallic carbon nanotubes, *Phys. Rev. B.* **58**, R16016–R16019, (1998).

30. J. G. Duque, H. Chen, A. K. Swan, A. P. Shreve, S. Kilina, S. Tretiak, X. Tu, M. Zheng, and S. K. Doorn, Violation of the condon approximation in semiconducting carbon nanotubes, *ACS Nano.* **5**, 5233–5241, (2011).

31. L. G. Moura, M. V. O. Moutinho, P. Venezuela, C. Fantini, A. Righi, M. S. Strano, and M. A. Pimenta, Raman excitation profile of the G band in single-chirality carbon nanotubes, *Phys. Rev. B.* **89**, 035402–1–035402–5, (2014).

32. H. Ajiki and T. Ando, Aharonov-Bohm effect in carbon nanotubes, *Physica B.* **201**, 349–352, (1994).

33. G. S. Duesberg, I. Loa, M. Burghard, K. Syassen, and S.Roth, Polarized Raman spectroscopy on isolated single-wall carbon nanotubes, *Phys. Rev. Lett.* **85**, 5436–5439, (2000).

34. H. H. Gommans, J. W. Alldredge, H. Tashiro, J. Park, J. Magnuson, and A. G. Rinzler, Fibers of aligned single-walled carbon nanotubes: Polarized Raman spectroscopy, *J. Appl. Phys.* **88**, 2509–2514, (2000).

35. L. Liu and S. Fan, Isotope labeling of carbon nanotubes and formation of ^{12}C-^{13}C nanotube junctions, *J. Am. Chem. Soc.* **123**, 11502–11503, (2001).

36. S. D. Costa, C. Fantini, A. Righi, A. Bachmatiuk, M. H. Rummeli, R. Saito, and M. A. Pimenta, Resonant Raman spectroscopy on enriched 13c carbon nanotubes, *Carbon.* **49**, 4719–4723, (2011).

37. L. G. Cançado, M. A. Pimenta, R. Saito, A. Jorio, L. O. Ladeira, A. Grueneis, A. G. Souza, G. Dresselhaus, and M. S. Dresselhaus, Stokes and anti-Stokes double resonance Raman scattering in two-dimensional graphite, *Phys. Rev. B.* **66**, 035415–1–035415–5, (2002).

38. R. Saito, A. Jorio, A. G. Souza, G. Dresselhaus, M. S. Dresselhaus, and M. A. Pimenta, Probing phonon dispersion relations of graphite by double resonance Raman scattering, *Phys. Rev. Lett.* **88**, 027401–1–027401–4, (2002).

39. M. Lucchese, F. Stavale, E. M. Ferreira, C. Vilani, M. Moutinho, R. B. Capaz, C. Achete, and A. Jorio, Quantifying ion-induced defects and Raman relaxation length in graphene, *Carbon.* **48**, 1592–1597, (2010).

40. R. Pfeiffer, H. Kuzmany, F. Simon, S. N. Bokova, and E. Obraztsova, Resonance Raman scattering from phonon overtones in double-wall carbon nanotubes, *Phys. Rev. B.* **71**, 155409–1–15540–8, (2005).

41. C. Fantini, A. Jorio, M. Souza, M. S. Strano, M. S. Dresselhaus, and M. A. Pimenta, Optical transition energies for carbon nanotubes from resonant Raman spectroscopy: Environment and temperature effects, *Phys. Rev. Lett.* **93**, 147406–1–147406–4, (2004).

42. G. D. Mahan, Oscillationsions of a thin hollow cylinder: Carbon nanotubes, *Phys. Rev. B.* **65**, 235402–1–235402–7, (2002).

43. V. Perebeinos and J. Tersoff, Valence force model for phonons in graphene and carbon nanotubes, *Phys. Rev. B.* **79**, 241409–1–241409–4, (2009).

44. J. Jiang, R. Saito, K. Sato, J. S. Park, G. G. Samsonidze, A. Jorio, G. Dresselhaus, and M. S. Dresselhaus, Exciton-photon, exciton-phonon matrix elements, and resonant Raman intensity of single-wall carbon nanotubes, *Phys. Rev. B.* **75**, 035405–1–035405–10, (2007).

45. P. T. Araujo, S. K. Doorn, S. Kilina, S. Tretiak, E. Einarsson, S. Maruyama, H. Chacham, M. A. Pimenta, and A. Jorio, Third and fourth optical transitions in

20

semiconducting carbon nanotubes, *Phys. Rev. Lett.* **98**, 067401–1–067401–4, (2007).

46. H. Telg, J. Maultzsch, S. Reich, F. Hennrich, and C. Thomsen, Raman intensities of the first optical transitions in carbon nanotubes, *phys. stat. sol. (b).* **243**, 3181–3185, (2006).

47. A. Jorio, C. Fantini, M. Pimenta, R. Capaz, G. Samsonidze, G. Dresselhaus, M. Dresselhaus, J. Jiang, N. Kobayashi, A. Gruneis, and R. Saito, Resonance Raman spectroscopy (n,m)-dependent effects in small-diameter single-wall carbon nanotubes, *Phys. Rev. B.* **71**, 075401–1–075401–11, (2005).

48. T. Michel, M. Paillet, J. Meyer, V. Popov, L. Henrard, P. Poncharal, A. Zahab, and J. Sauvajol, Raman spectroscopy of (n, m)-identified individual single-walled carbon nanotubes, *Phys. Status Solidi B.* **244**, 3986–3991, (2007).

49. H. Kataura, Y. Kumazawa, Y. Maniwa, I. Umezu, S. Suzuki, Y. Ohtsuka, and Y. Achiba, Optical properties of single-wall carbon nanotubes, *Synth. Met.* **103**, 2555–2558, (1999).

50. J. C. Charlier and P. Lambin, Electronic structure of carbon nanotubes with chiral symmetry, *Phys. Rev. B.* **57**, R15037–R15039, (1998).

51. G. G. Samsonidze, R. Saito, N. Kobayashi, A. Gruneis, J. Jiang, A. Jorio, S. G. Chou, G. Dresselhaus, and M. S. Dresselhaus, Family behavior of the optical transition energies in single-wall carbon nanotubes of smaller diameters, *Appl. Phys. Lett.* **85**, 5703–5705, (2004).

52. L. Yang and J. Han, Electronic structure of deformed carbon nanotubes, *Phys. Rev. Lett.* **85**, 154–157, (2000).

53. P. T. Araujo and A. Jorio, The role of environmental effects on the optical transition energies and radial breathing mode frequency of single wall carbon nanotubes, *phys. stat. sol. (b).* **245**, 2201–2204, (2008).

54. S. Chiashi, K. Kono, D. Matsumoto, J. Shitaba, N. Homma, A. Beniya, T. Yamamoto, and Y. Homma, Adsorption effects on radial breathing mode of single-walled carbon nanotubes, *Phys. Rev. B.* **91**, 155415–1–155415–5, (2015).

55. R. Saito, M. Fujita, G. Dresselhaus, and M. S. Dresselhaus, Electronic structure of chiral graphene tubules, *Appl. Phys. Lett.* **60**, 2204–2206, (1992).

56. R. Saito, T. Takeya, T. Kimura, G. Dresselhaus, and M. S. Dresselhaus, Raman intensity of single-wall carbon nanotubes, *Phys. Rev. B.* **57**, 4145–4153, (1998).

57. K. Kato and S. Saito, Geometries, electronic structures and energetics of small-diameter single-walled carbon nanotubes, *Physica E: Low-dimensional Systems and Nanostructures.* **43**, 669–672, (2011).

58. K. Liu, W. Wang, M. Wu, F. Xiao, X. Hong, S. Aloni, X. Bai, E. Wang, and F. Wang, Intrinsic radial breathing oscillation in suspended single-walled carbon nanotubes, *Phys. Rev. B.* **83**, 113404–1–113404–4, (2011).

59. P. T. Araujo, I. O. Maciel, P. B. C. Pesce, M. A. Pimenta, S. K. Doorn, H. Qian, A. Hartschuh, M. Steiner, L. Grigorian, K. Hata, and A. Jorio, Nature of the constant factor in the relation between radial breathing mode frequency and tube diameter for single-wall carbon nanotubes, *Phys. Rev. B.* **77**, 241403(R)–1–241403(R)–4, (2008).

60. E. Einarsson, H. Shiozawa, C. Kramberger, M. H. Rummeli, A. Gruneis, T. Pichler, and S. Maruyama, Revealing the small-bundle interal structure of vertically aligned single-walled carbon nanotube films, *J. Phys. Chem. C.* **111**, 17861–17864, (2007).

61. A. Jorio, R. Saito, J. H. Hafner, C. M. Lieber, M. Hunter, T. McClure, G. Dresselhaus, and M. S. Dresselhaus, Structural (n, m) determination of isolated single-wall carbon nanotubes by resonant Raman scattering, *Phys. Rev. Lett.* **86**, 1118–1121, (2001).

62. S. Bandow, S. Asaka, Y. Saito, A. M. Rao, L. Grigorian, E. Richter, and P. C. Eklund, Effect of the growth temperature on the diameter distribution and chirality of single-

wall carbon nanotubes, *Phys. Rev. Lett.* **80**, 3779–3782, (1998).

63. Y. Homma, S. Chiashi, T. Yamamoto, K. Kono, D. Matsumoto, J. Shitaba, and S. Sato, Photoluminescence measurements and molecular dynamics simulations of water adsorption on the hydrophobic surface of a carbon nanotube in water vapor, *Phys. Rev. Lett.* **110**, 157402–1–157402–4, (2013).

64. S. M. Bachilo, M. B. Strano, C. Kittrell, R. H. Hauge, R. E. Smalley, and R. B. Weisman, Structure-assigned optical spectra of single-walled carbon nanotubes, *Science.* **298**, 2361–2366, (2002).

65. H. Telg, J. Maultzsch, S. Reich, F. Hennrich, and C. Thomsen, Chirality distribution and transition energies of carbon nanotubes, *Phys. Rev. Lett.* **93**, 177401–1–177401–4, (2004).

66. J. Maultzsch, H. Telg, S. Reich, and C. Thomsen, Radial breathing mode of single-walled carbon nanotubes: Optical transition energies and chiral-index assignment, *Phys. Rev. B.* **72**, 205438–1–205438–16, (2005).

67. M. Paillet, T. Michel, J. C. Meyer, V. N. Popov, L. Henrard, S. Roth, and J. L. Sauvajol, Raman active phonons of identified semiconducting single-walled carbon nanotubes, *Phys. Rev. Lett.* **96**, 257401–1–257401–4, (2006).

68. J. Soares, A. P. M. Barboza, P. T. Araujo, N. M. B. Neto, D. Nakabayashi, N. Shadmi, T. S. Yarden, A. Ismach, N. Geblinger, E. Joselevich, C. Vilani, L. G. Cançado, L. Novotny, G. Dresselhaus, M. S. Dresselhaus, B. R. A. Neves, M. S. C. Mazzoni, and A. Jorio, Modulating the electronic properties along carbon nanotubes via tube-substrate interaction, *Nano Lett.* **10**, 5043–5048, (2010).

69. Y. Y. Zhang, H. Son, J. Zhang, M. S. Dresselhaus, J. Kong, and Z. F. Liu, Raman spectra variation of partially suspended individual single-walled carbon nanotubes, *J. Phys. Chem. C.* **111**, 1983–1987, (2007).

70. R. Kumar, M. Aykol, and S. B. Cronin, Effect of nanotube-nanotube coupling on the radial breathing mode of carbon nanotubes, *Phys. Rev. B.* **78**, 165428–1–165428–4, (2008).

71. S. Chiashi, S. Watanabe, T. Hanashima, and Y. Homma, Influence of gas adsorption on optical transition energies of single-walled carbon nanotubes, *Nano Lett.* **8**, 3097–3101, (2008).

72. A. P. Shreve, E. H. Haroz, S. M. Bachilo, R. B. Weisman, S. Tretiak, S. Kilina, and S. K. Doorn, Determination of exciton-phonon coupling elements in single-walled carbon nanotubes by Raman overtone analysis, *Phys. Rev. Lett.* **98**, 037405–1–037405–4, (2007).

73. T. Ando, Excitons in carbon nanotubes, *J. Phys. Soc. Jpn.* **66**, 1066–1073, (1997).

74. O. Kiowski, S. Lebedkin, F. Hennrich, S. Malik, H. Rosner, K. Arnold, C. Surgers, and M. M. Kappes, Photoluminescence microscopy of carbon nanotubes grown by chemical vapor deposition: Influence of external dielectric screening on optical transition energies, *Phys. Rev. B.* **75**, 075421–1–075421–7, (2007).

75. Y. Ohno, S. Iwasaki, Y. Murakami, S. Kishimoto, S. Maruyama, and T. Mizutani, Chirality-dependent environmental effects in photoluminescence of single-walled carbon nanotubes, *Phys. Rev. B.* **73**, 235427–1–235427–5, (2006).

76. J. Lefebvre and P. Finnie, Photoluminescence and förster resonance energy transfer in elemental bundles of single-walled carbon nanotubes, *J. Phys. Chem. C.* **113**, 7536–7540, (2009).

77. K. Arnold, S. Lebedkin, O. Kiowski, F. Hennrich, and M. M. Kappes, Matrix-imposed stress-induced shifts in the photoluminescence of single-walled carbon nanotubes at low temperatures, *Nano Lett.* **4**, 2349–2354, (2004).

78. N. R. Raravikar, P. Keblinski, A. M. Rao, M. S. Dresselhaus, L. S. Schadler, and

22

P. M. Ajayan, Temperature dependence of radial breathing mode Raman frequency of single-walled carbon nanotubes, *Phys. Rev. B.* **66**, 235424–1–235424–9, (2002).

79. Z. P. Zhou, L. Ci, L. Song, X. Q. Yan, D. F. Liu, H. J. Yuan, Y. Gao, J. X. W. andL. F. Liu, W. Y. Zhou, S. S. Xie, Y. X. Du, and Y. J. Mo, The intrinsic temperature effect of Raman spectra of double-walled carbon nanotubes, *Chem. Phys. Lett.* **396**, 372–376, (2004).

80. S. Chiashi, Y. Murakami, Y. Miyauchi, and S. Maruyama, Temperature dependence of Raman scattering from single-walled carbon nanotubes: Undefined radial breathing mode peaks at high temperatures, *Jpn. J. Appl. Phys.* **47**, 2010–2015, (2008).

81. S. B. Cronin, Y. Yin, A. Walsh, R. B. Capaz, A. Stolyarov, P. Tangney, M. L. Cohen, S. G. Louie, A. K. Swan, M. S. Unlu, B. B. Goldberg, and M. Tinkham, Temperature dependence of the optical transition energies of carbon nanotubes: The role of electron-phonon coupling and thermal expansion, *Phys. Rev. Lett.* **96**, 127403–1–127403–4, (2006).

82. J. Lefebvre, P. Finnie, and Y. Homma, Temperature-dependent photoluminescence from single-walled carbon nanotubes, *Phys. Rev. B.* **70**, 045419–1–045419–8, (2004).

83. K. Yoshino, T. Kato, Y. Saito, J. Shitaba, T. Hanashima, K. Nagano, S. Chiashi, and Y. Homma, Temperature distribution and thermal conductivity measurements of chirality-assigned single-walled carbon nanotubes by photoluminescence imaging spectroscopy, *ACS Omega.* **3**, 4352–4356, (2018).

84. H. D. Li, K. T. Yue, Z. L. Lian, Y. Zhan, L. X. Zhou, S. L. Zhang, Z. J. Shi, Z. N. Gu, B. B. Liu, R. S. Yang, H. B. Yang, G. T. Zou, Y. Zhang, and S. Iijima, Temperature dependence of the Raman spectra of single-wall carbon nanotubes, *Appl. Phys. Lett.* **76**, 2053–2055, (2000).

85. K. Liu, X. Hong, S. Choi, C. Jin, R. Capaz, J. Kim, W. Wang, X. Bai, S. G. Louie, E. Wang, and F. Wang, Systematic determination of absolute absorption cross-section of individual carbon nanotubes, *Proc. Natl. Acad. Sci. U.S.A.* **111**, 7564–7569, (2014).